Solid-State Electronics 228 (2025) 109135

Contents lists available at ScienceDirect

Solid State Electronics

journal homepage: www.elsevier.com/locate/sse

Optimizing unconventional trilayer SOTs for field-free switching☆

Nils Petter Jørstad [a,*], Wolfgang Goes [c], Siegfried Selberherr [b], Viktor Sverdlov [a,b]

[a] Christian Doppler Laboratory for Nonvolatile Magnetoresistive Memory and Logic at the Institute for Microelectronics, TU Wien, Gußhausstraße 27-29/E360, 1040 Vienna, Austria
[b] Institute for Microelectronics, TU Wien, Gußhausstraße 27-29, A-1040, Vienna, Austria
[c] Silvaco Europe Ltd., Compass Point, St Ives, PE27 5JL, Cambridge, United Kingdom

ARTICLE INFO

The review of this paper was arranged by Francisco F. Gamiz

Keywords:
Anomalous Hall effect
Anisotropic magnetroresistance
Rashba–Edelstein effect
SOT-MRAM

ABSTRACT

The symmetry and magnitude of unconventional spin–orbit torques in ferromagnet/heavy metal/ferromagnet trilayers are investigated. Several spin-generating mechanisms are considered such as the anomalous Hall effect, anisotropic magnetoresistance, the Rashba–Edelstein effect, and the spin Hall effect. Optimal material thicknesses and magnetization configurations for maximizing out-of-plane spin torques for breaking the bilayer symmetry are presented. Furthermore, field-free switching simulations of a perpendicular SOT-MRAM utilizing the optimized trilayer torques are demonstrated, showing improved switching currents compared to another reported trilayer-based device.

1. Introduction

Spin–orbit torques (SOT) enable rapid and energy-efficient manipulation of magnetic states in emerging spintronic devices [1–3]. Conventional SOTs, generated through the spin Hall effect (SHE) in the bulk and the Rashba–Edelstein effect (REE) at the interface in heavy metal (HM)/ ferromagnetic (FM) bilayers have proven to be successful in switching logical states in SOT magnetoresistive random access memory (SOT-MRAM) [4–6]. The logical state is stored in the relative magnetization orientation of two magnetic layers called the free layer (FL) and the reference layer (RL), separated by a tunnel barrier (TB) forming a magnetic tunneling junction (MTJ). These devices can achieve sufficiently high densities to challenge conventional memories such as SRAM by utilizing perpendicular magnetic anisotropy [7,8]. However, due to the symmetry of conventional SOTs, reversing a perpendicular magnetic state is challenging without additional assistance, such as an external magnetic field [2,3,8]. A promising approach involves leveraging unconventional SOTs in FM/NM/FM trilayers to break this symmetry [9–11]. By introducing a second FM layer below the NM, additional spin currents can be obtained through spin–orbit coupling (SOC) in the FM bulk and the FM/NM interface, offering enhanced control over the resulting SOTs compared to bilayers [12,13].

We investigate unconventional SOTs in trilayers to identify optimal configurations for achieving field-free switching of perpendicularly magnetized FM layers. We consider a FePt/W/CoFeB trilayer with an in-plane electrical current and in-plane CoFeB magnetization perpendicular to the current, a direction along which the bilayer torques vanish due to their symmetry. In the FePt bulk, spin currents are generated through the anomalous Hall effect (AHE) and anisotropic magnetoresistance (AMR) [14]. We consider the SHE in the bulk of the W layer, and we compute the spin currents generated through the REE by considering spin-dependent scattering from a Rashba SOC potential at the W/FM interfaces. We include the four spin current contributions in a spin drift–diffusion model and calculate the SOTs acting on the CoFeB layer.

Combining the drift–diffusion model with the Landau-Lifshitz-Gilbert (LLG) equation allows modeling of the magnetization dynamics. We investigate the magnetization dynamics in a CoFeB/W/CoFeB trilayer-based SOT-MRAM cell, optimized for maximizing the trilayer torques from the REE. We demonstrate deterministic field-free switching and improved performance compared to a similar reported device [10].

2. Micromagnetic model

The magnetization dynamics are described by the LLG equation:

$$\frac{\partial \mathbf{m}}{\partial t} = -\gamma \mu_0 \mathbf{m} \times \mathbf{H}_{\text{eff}} + \alpha \mathbf{m} \times \frac{\partial \mathbf{m}}{\partial t} + \frac{1}{M_S} \mathbf{T}_{\mathbf{S}} \tag{1}$$

$\boldsymbol{m} = \boldsymbol{M}/M_S$ is the normalized magnetization, M_S is the saturation magnetization. γ is the gyromagnetic ratio, μ_0 is the permeability of vacuum, and α is the Gilbert damping constant. The first term describes the precession of the magnetization around an effective magnetic field $\boldsymbol{H}_{\text{eff}}$, the second term describes the damping of the magnetization towards this field, and the third term describes the spin

☆ The review of this paper was arranged by Francisco F. Gamiz.
* Corresponding author.
E-mail address: jorstad@iue.tuwien.ac.at (N.P. Jørstad).

https://doi.org/10.1016/j.sse.2025.109135

Available online 2 May 2025

torques $\mathbf{T_S}$ acting on the magnetization. The effective field consists of several important contributions, such as the exchange field, demagnetization field, anisotropy field, and the interfacial Dzyaloshinskii–Moriya interaction [15]:

$$\mathbf{H}_{\text{eff}} = \mathbf{H}_{\text{exch}} + \mathbf{H}_{\text{demag}} + \mathbf{H}_{\text{aniso}} + \mathbf{H}_{\text{iDMI}} \tag{2}$$

The spin torque is obtained from the non-equilibrium spin accumulation $\boldsymbol{S}$ transverse to the magnetization [16]:

$$\mathbf{T_S} = -\frac{D_e}{\lambda_J^2}\mathbf{m}\times\mathbf{S} - \frac{D_e}{\lambda_\phi^2}\mathbf{m}\times(\mathbf{m}\times\mathbf{S}) \tag{3}$$

λ_J and λ_ϕ are exchange and dephasing lengths, respectively, while D_e is the electron diffusion coefficient.

3. Spin drift-diffusion model

The non-equilibrium spin accumulation is obtained by solving its continuity equation for a steady state [16]:

$$\frac{\partial \mathbf{S}}{\partial t} = 0 = -\nabla\tilde{J}_S - D_e\left(\frac{\mathbf{S}}{\lambda_{sf}^2} + \frac{\mathbf{S}\times\mathbf{m}}{\lambda_J^2} + \frac{\mathbf{m}\times(\mathbf{S}\times\mathbf{m})}{\lambda_\varphi^2}\right) \tag{4}$$

$(\tilde{J}_S)_{ij}$ is the spin polarization current density in units of A/s, with direction j and polarization i, and λ_{sf} is the spin-flip length.

The spin polarization current density is described by the diffusion of spin accumulation, the flow of spins carried by an electrical current polarized by the local magnetization [17]:

$$\tilde{J}_S = -D_e\nabla\boldsymbol{S} - \frac{\mu_B}{e}\beta_\sigma\mathbf{m}\otimes\left(\mathbf{J_C} - \frac{e}{\mu_B}\beta_D D_e(\nabla\boldsymbol{S})^{\mathrm{T}}\mathbf{m}\right) \tag{5}$$

$\mathbf{J_C} = \sigma\mathbf{E}$ is the electrical current density from the applied field $\mathbf{E}$, where σ is the electrical conductivity. The applied electrical field is given by $\mathbf{E} = -\nabla V$, where V is the electrical potential, obtained from solving $\nabla\cdot\mathbf{J_C} = 0$ with Dirichlet boundary conditions for the applied voltage at the contacts. β_σ and β_D are the dimensionless electrical current polarization and diffusion spin polarization, respectively. μ_B is the Bohr magneton and e is the elementary charge.

At external boundaries not containing contacts, we assume zero flux of spin and electrical currents, i.e., $(J_S)_{ij}n_j = 0$ and $\mathbf{J_C}\cdot\mathbf{n} = 0$, where $\mathbf{n}$ is the interface normal. At internal interfaces, we use the boundary conditions from the magnetoelectronic circuit theory [16].

In HMs, the spin current from the SHE flows perpendicularly to the electrical field with a polarization perpendicular to both [16]:

$$\tilde{J}_S^{\text{SHE}} = -\theta_{\text{SH}}\frac{\mu_B}{e}\epsilon\mathbf{J_C} \tag{6}$$

$\theta_{\text{SH}} = \sigma_{\text{SH}}/\sigma$ is the dimensionless spin Hall angle, which captures the efficiency of the charge to spin current conversion, where σ_{SH} is the spin Hall conductivity. ϵ_{ijk} is the Levi-Civita tensor.

In FMs, the spin current from the AHE is polarized along $\mathbf{m}$ and flows along $\mathbf{m}\times\mathbf{E}$ [12]:

$$\tilde{J}_S^{\text{AHE}} = -\theta_{\text{AH}}\frac{\mu_B}{e}\mathbf{m}\otimes(\mathbf{m}\times\mathbf{J_C}) \tag{7}$$

θ_{AH} is the anomalous Hall angle.

The AMR spin current is also polarized along $\mathbf{m}$ with the direction given by $\mathbf{m}(\mathbf{m}\cdot\mathbf{E})$ [12]:

$$\tilde{J}_S^{\text{AMR}} = -\theta_{\text{AMR}}\frac{\mu_B}{e}\mathbf{m}\otimes\mathbf{m}(\mathbf{m}\cdot\mathbf{J_C}) \tag{8}$$

θ_{AMR} is the AMR angle.

At HM/FM interfaces, the REE is captured by boundary conditions for the spin current at either side of the interface [15,18]:

$$\tilde{J}_S^{\text{REE}}\mathbf{n}|_{\text{HM}} = -\frac{\mu_B}{e}\frac{\boldsymbol{\sigma}_{\mathbf{S}}^{\mathbf{HM}}(\boldsymbol{m},\boldsymbol{E})}{\sigma}J_C^{\text{ip}} \tag{9}$$

$$\tilde{J}_S^{\text{REE}}\mathbf{n}|_{\text{FM}} = -\frac{\mu_B}{e}\frac{\boldsymbol{\gamma}_{\mathbf{S}}^{\mathbf{FM}}(\boldsymbol{m},\boldsymbol{E})}{\sigma}J_C^{\text{ip}} \tag{10}$$

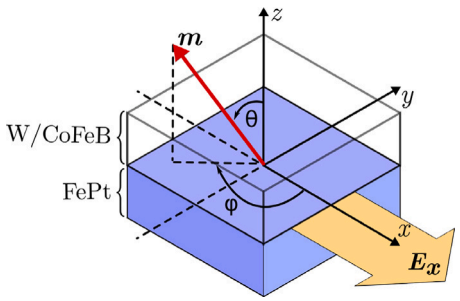

Fig. 1. A sketch of the FePt/W/CoFeB trilayer geometry considered, where θ and ϕ are the polar and azimuthal angles of the FePt magnetization direction, respectively. $\mathbf{E}_\mathbf{x}$ is an applied electric field along the x direction.

J_C^{ip} is the magnitude of the in-plane current at the interface. $\boldsymbol{\sigma}_{\mathbf{S}}^{\mathbf{HM}}$ and $\boldsymbol{\gamma}_{\mathbf{S}}^{\mathbf{FM}}$ are interfacial conductivity tensors computed by considering quantum mechanical scattering of a Rashba SOC and exchange potential at the interface [15]. The spin torque due to the exchange interaction at the interface is given by

$$\mathbf{T}_{\mathbf{S}}^{\text{int}} = -\frac{\mu_B}{e}\frac{\boldsymbol{\gamma}_{\mathbf{S}}^{\mathbf{mag}}(\boldsymbol{m},\boldsymbol{E})}{\sigma}J_C^{\text{ip}}\delta(z), \tag{11}$$

for an interface at $z = 0$, where $\boldsymbol{\gamma}_{\mathbf{S}}^{\mathbf{mag}}$ is the interface torkivity tensor [18].

The spin currents from the SHE, AHE, AMR, and REE are included as additional contributions to Eq. (5). All of the considered spin-generating effects have a reciprocal effect on the charge current density, which are assumed to weakly affect the resulting spin accumulation and torques and are, therefore, not considered in this work.

4. Trilayer SOTs

We consider a FePt(d_{FePT})/W(d_{W})/CoFeB(1.2 nm) trilayer system with an in-plane electrical current density of 10^{12} A/m^2, where d_{FePT} and d_{W} is the FePt and W thickness, respectively. We keep the CoFeB magnetization fixed along $\hat{\mathbf{z}}\times\mathbf{E}$, where the bilayer torques from the SHE and REE vanish, leaving only the contribution from the trilayer torques. The system is depicted in Fig. 1, where the polar and azimuthal angles describe the FePt magnetization direction. FePt exhibits the AHE and AMR with reported Hall angles of approximately 0.25 and −0.015 [12,14], respectively. It has been widely reported that W has a large spin Hall angle of approximately −0.3 in its high resistance β phase [19]. Due to the strong SOC in W, we consequently assume a strong REE is present at the W/FM interfaces. We solve the drift–diffusion equations for this system and analyze the resulting out-of-plane torques acting on the CoFeB layer, as these torques bring the magnetization out-of-plane and break the symmetry of the conventional torques.

Fig. 2 shows the thickness dependence of out-of-plane spin torques on the FePt and W thickness. As the trilayer spin currents originating from the FePt and FePt/W interface diffuse due to bulk spin-flip processes, a HM thickness below the spin-diffusion length is necessary to maximize their contribution (2.4 nm in W [20]). The opposite is generally desired in HM/FM bilayers as the anti-damping torques increase with the HM thickness up to a saturation point [21]. Therefore, the trilayer contribution from the SHE peaks at thicknesses near the spin-diffusion length as the total SHE spin current increases with the HM thickness, while the SHE spin current scattered from the bottom FM decreases with the thickness. Consequently, the HM thickness significantly affects which contribution dominates.

For increasing FePt thickness, we observe that the REE contribution remains constant, while the SHE contribution increases for decreasing thickness and saturates with increasing thickness. Similarly to the SHE torques in bilayers, we observe that AHE and AMR torques increase with the FePt thickness, reaching saturation points based on the spin-diffusion length (5 nm in FePt [12]).

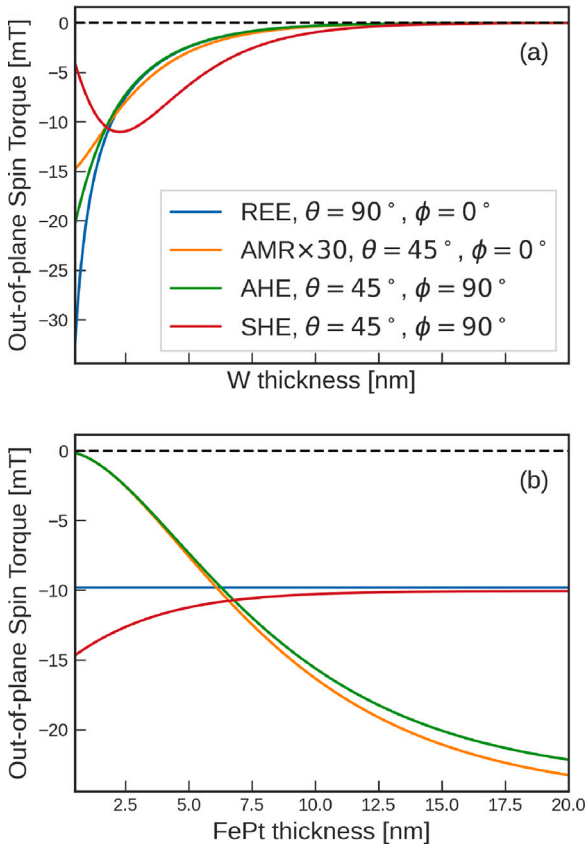

Fig. 2. Thickness dependence of the out-of-plane unconventional SOTs acting on the CoFeB magnetization in a FePt/W/CoFeB(1.2 nm) trilayer. Panel (a): The thickness of W is varied while FePt thickness is fixed at 6 nm. Panel (b): W thickness is fixed at 2 nm, and the FePt thickness is varied. FePt magnetization directions, which maximize the resulting torques, are chosen.

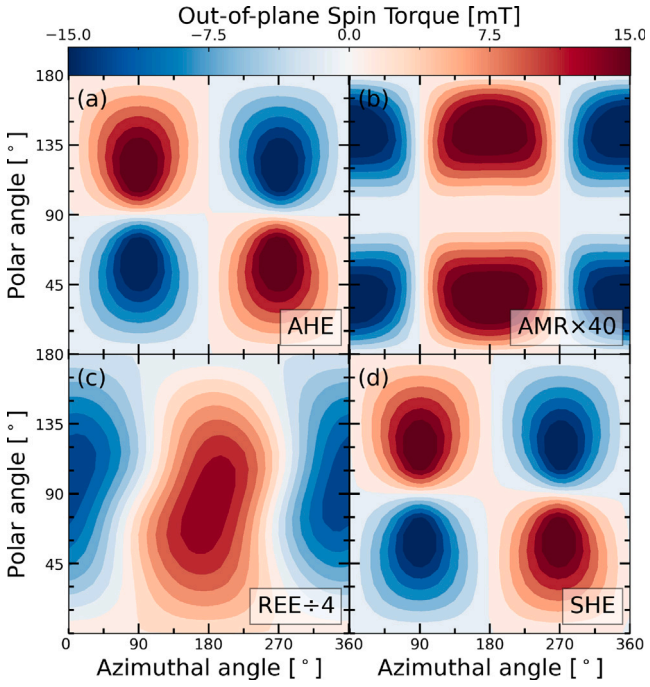

Fig. 3. Angular dependence of the out-of-plane unconventional SOTs acting on the CoFeB magnetization in a FePt(6 nm)/W(2 nm)/CoFeB(1.2 nm) trilayer. The CoFeB magnetization points along $-y$, where the conventional bilayer torques vanish. Panels (a), (b), (c), and (d) show the spin torque contribution from the AHE, AMR, REE, and SHE, respectively.

Fig. 3 shows the dependence of the out-of-plane SOTs on the FePt magnetization direction, revealing a strong angular dependence of the torques. In particular, the REE is most pronounced, when the magnetization aligns with the current direction, suggesting it could be the dominating mechanism for magnetization reversal in CoFeB/Ti/CoFeB trilayers [11]. The AHE and SHE have a similar angular dependence, where a 45° tilted magnetization orthogonal to the current direction is preferred for maximizing their contribution. The AMR contribution is also the most pronounced, when the magnetization is tilted by 45°, however, it is the strongest in the x-z plane.

5. Field-free switching with trilayer SOTs

Combining the drift–diffusion and the LLG equation and solving them together with the finite element method, enables simulations of the magnetization dynamics during switching of the FL. We consider a CoFeB/W SOT line with a width of 70 nm, below a CoFeB(FL)/MgO(TB)/CoFeB(RL) perpendicular MTJ with a diameter of 60 nm, and simulate the switching of the FL from the antiparallel to the parallel state. To represent a typical SOT-MTJ, we consider a thickness of 1.2 nm for the FL, and 1.0 nm for the TB and the RL [2,3,7].

The magnetization of the bottom CoFeB layer is fixed along the current direction to maximize the REE contribution. To focus on the effects of unconventional torques on switching performance, we aim to minimize any interlayer effects between the bottom CoFeB layer and the FL. Since the unconventional torques originating from the REE are independent of the bottom layer's thickness, we consider a thickness of 4.0 nm, as used in [22], where it was reported that the stray field did not strongly influence the switching.

To optimize the unconventional torques from the REE, a thin W layer with a thickness below the diffusion length is necessary, as shown in Fig. 2a. However, thicknesses below 1.0 nm can induce a strong interlayer exchange coupling (IEC) between the bottom CoFeB and the FL [23]. Although this could be beneficial, it falls outside the scope of our study. Therefore, we will use a W thickness of 1.0 nm to ensure a strong REE contribution while eliminating the need to account for the IEC.

Fig. 4 shows the evolution of the FL magnetization over time for various applied currents. For all the applied currents, we observe field-free switching and similar dynamics: The magnetization is quickly switched halfway, and thereafter, damped oscillations bring the magnetization to the fully switched configuration. With increasing current magnitude the oscillations decrease in amplitude and relax faster.

Assuming that switching off the current after the average z-component of the normalized magnetization reaches -0.75 guarantees that the magnetization relaxes to the fully switched state. Thus, we can roughly estimate the required switching current pulse width. Fig. 5 shows the switching current as a function of the inverse switching pulse width. We compare our results with the ones from a previously reported similar trilayer device [10]. The simulation results of our proposed SOT-MTJ configuration suggest a drastic decrease in the required switching current.

6. Conclusion

In conclusion, we demonstrate that FM/HM/FM trilayers can generate unconventional SOTs acting on the upper FM layer, which are tunable by the lower FM magnetization direction. Our spin drift–diffusion approach enables the study and optimization of SOTs concerning materials, layer thickness, and magnetization directions. Ultimately, coupling the computed torques with the Landau–Lifshitz–Gilbert equation is essential for investigating the resulting magnetization dynamics to demonstrate deterministic field-free switching. With optimized unconventional SOTs our simulations of the resulting dynamics demonstrate a structure which promises a drastic reduction in switching currents compared to similar devices.

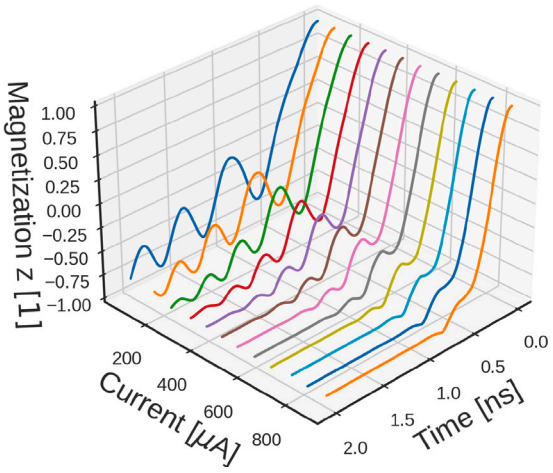

Fig. 4. Average z-component of the FL magnetization in a CoFeB(4 nm)/W(1 nm)/[CoFeB(1.2 nm)/MgO (1 nm)/CoFeB(1 nm)] SOT-MTJ as a function of time ([·] denotes the MTJ part of the stack), for various applied currents.

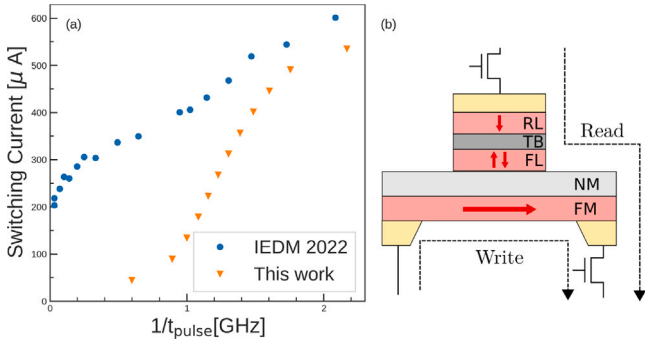

Fig. 5. (a): Switching time as a function of the inverse switching current pulse width, for the same system as in Fig. 4. (b): A schematic of the trilayer SOT-MTJ system considered.

CRediT authorship contribution statement

Nils Petter Jørstad: Writing – review & editing, Writing – original draft, Software, Investigation, Data curation, Conceptualization. **Wolfgang Goes:** Writing – review & editing, Software. **Siegfried Selberherr:** Writing – review & editing, Supervision. **Viktor Sverdlov:** Writing – review & editing, Supervision, Project administration, Funding acquisition, Conceptualization.

Declaration of competing interest

The authors declare the following financial interests/personal relationships which may be considered as potential competing interests: Nils Petter Joerstad reports financial support was provided by Christian Doppler Research Association. If there are other authors, they declare that they have no known competing financial interests or personal relationships that could have appeared to influence the work reported in this paper.

Acknowledgments

The financial support by the Federal Ministry of Labour and Economy, the National Foundation for Research, Technology and Development, and the Christian Doppler Research Association is gratefully acknowledged. The authors acknowledge TU Wien Bibliothek for financial support through its Open Access Funding Program.

Data availability

Data will be made available on request.

References

[1] Cao Y, Xing G, Lin H, Zhang N, Zheng H, Wang K. Prospect of spin-orbitronic devices and their applications. IScience 2020;23(10):101614.
[2] Han X, Wang X, Wan C, Yu G, Lv X. Spin-orbit torques: Materials, physics, and devices. Appl Phys Lett 2021;118(12):120502.
[3] Nguyen V, Rao S, Wostyn K, Couet S. Recent progress in spin-orbit torque magnetic random-access memory. Npj Spintron 2024;2(1):48.
[4] Miron IM, Garello K, Gaudin G, Zermatten P-J, Costache MV, Auffret S, et al. Perpendicular switching of a single ferromagnetic layer induced by in-plane current injection. Nature 2011;476:189–93.
[5] Liu L, Lee OJ, Gudmundsen TJ, Ralph DC, Buhrman RA. Current-induced switching of perpendicularly magnetized magnetic layers using spin torque from the spin Hall effect. Phys Rev Lett 2012;109:096602.
[6] Garello K, Yasin F, Couet S, Souriau L, Swerts J, Rao S, et al. SOT-MRAM 300MM integration for low power and ultrafast embedded memories. In: 2018 IEEE symposium on VLSI circuits. 2018, p. 81–2.
[7] Ikeda S, Miura K, Yamamoto H, Mizunuma K, Gan H, Endo M, et al. A perpendicular-anisotropy CoFeB–MgO magnetic tunnel junction. Nat Mater 2010;9:721–4.
[8] Krizakova V, Perumkunnil M, Couet S, Gambardella P, Garello K. Spin-orbit torque switching of magnetic tunnel junctions for memory applications. J Magn Magn Mater 2022;562:169692.
[9] Ryu J, Thompson R, Park JY, Kim S-J, Choi G, Kang J, et al. Efficient spin–orbit torque in magnetic trilayers using all three polarizations of a spin current. Nat Electron 2022;5:217–23.
[10] Cai K, Talmelli G, Fan K, Van Beek S, Kateel V, Gupta M, et al. First demonstration of field-free perpendicular SOT-MRAM for ultrafast and high-density embedded memories. In: 2022 international electron devices meeting. IEDM, 2022, p. 36.2.1–4.
[11] Yang Q, Han D, Zhao S, Kang J, Wang F, Lee S-C, et al. Field-free spin–orbit torque switching in ferromagnetic trilayers at sub-ns timescales. Nat Commun 2024;15(1):1814.
[12] Taniguchi T, Grollier J, Stiles MD. Spin-transfer torques generated by the anomalous Hall effect and anisotropic magnetoresistance. Phys Rev Appl 2015;3:044001.
[13] Amin VP, Haney PM, Stiles MD. Interfacial spin-orbit torques. J Appl Phys 2020;128(15):151101.
[14] Seki T, Iihama S, Taniguchi T, Takanashi K. Large spin anomalous Hall effect in $L1_0$–FePt: Symmetry and magnetization switching. Phys Rev B 2019;100:144427.
[15] Jørstad NP, Fiorentini S, Ender J, Goes W, Selberherr S, Sverdlov V. Micromagnetic modeling of SOT-MRAM dynamics. Phys B 2024;676:415612.
[16] Haney PM, Lee H-W, Lee K-J, Manchon A, Stiles MD. Current induced torques and interfacial spin-orbit coupling: Semiclassical modeling. Phys Rev B 2013;87:174411.
[17] Fiorentini S, Bendra M, Ender J, L. de Orio R, Goes W, Selberherr S, et al. Spin and charge drift-diffusion in ultra-scaled MRAM cells. Sci Rep 2022;12:20958.
[18] Amin V, Stiles M. Spin transport at interfaces with spin-orbit coupling: Phenomenology. Phys Rev B 2016;94:104420.
[19] Pai C-F, Liu L, Li Y, Tseng HW, Ralph DC, Buhrman RA. Spin transfer torque devices utilizing the giant spin Hall effect of tungsten. Appl Phys Lett 2012;101(12):122404.
[20] Zhang W, Jungfleisch MB, Jiang W, Sklenar J, Fradin FY, Pearson JE, et al. Spin pumping and inverse spin Hall effects—Insights for future spin-orbitronics (invited). J Appl Phys 2015;117(17):172610.
[21] Zhu L, Ralph DC, Buhrman RA. Maximizing spin-orbit torque generated by the spin Hall effect of Pt. Appl Phys Rev 2021;8(3):031308.
[22] Baek S-hC, Amin VP, Oh Y-W, Go G, Lee S-J, Lee G-H, et al. Spin currents and spin–orbit torques in ferromagnetic trilayers. Nat Mater 2018;17(6):509–13.
[23] Liu S, Wan C, Feng J, Luo X, Zhang R, Namsaraev ZZ, et al. Magnetization switching driven by spin current in a T-type ferromagnetic trilayer. Appl Phys Lett 2024;124(19):192403.